Pharm Res (2019) 36: 66
https://doi.org/10.1007/s11095-019-2602-y

RESEARCH PAPER

Efficacy of Surface-Modified PLGA Nanoparticles as a Function of Cervical Cancer Type

Lee B. Sims[1] • Keegan C. Curry[2] • Sindhu Parupalli[1] • Gwynneth Horner[3] • Hermann B. Frieboes[1,4,5] • Jill M. Steinbach-Rankins[1,5,6,7]

Received: 14 January 2019 / Accepted: 4 March 2019 / Published online: 13 March 2019

ABSTRACT

Purpose Hypovascularization of cervical tumors, coupled with intrinsic and acquired drug resistance, has contributed to marginal therapeutic outcomes by hindering chemotherapeutic transport and efficacy. Recently, the heterogeneous penetration and distribution of cell penetrating peptide (CPP, here MPG) and polyethylene glycol (PEG) modified poly(lactic-co-glycolic acid) (PLGA) nanoparticles (NPs) were evaluated as a function of tumor type and morphology in cervical cancer spheroids modeling hypovascularized tumor nodules. Building upon this work, this study investigates the efficacy imparted by surface-modified Doxorubicin-loaded NPs transported into hypovascularized tissue.

Methods NP efficacy was measured in HeLa, CaSki, and SiHa cells. NP internalization and association, and associated cell viability, were determined in monolayer and spheroid models.

Results MPG and PEG-NP co-treatment was most efficacious in HeLa cells, while PEG NPs were most efficacious in CaSki cells. NP surface-modifications were unable to improve efficacy, relative to unmodified NPs, in SiHa cells.

Conclusions The results highlight the dependence of efficacy on tumor type and the associated microenvironment. The results further relate previous NP transport studies to efficacy, as a function of surface-modification and cell type. Longer-term, this information may help guide the design of NP-mediated strategies to maximize efficacy based on patient-specific cervical tumor origin and characteristics.

KEY WORDS 3D cell culture · cell penetrating peptide (CPP) · cervical cancer · nanoparticles · nanotherapy

Guest Editor: Joshua Reineke

Hermann B. Frieboes and Jill M. Steinbach-Rankins are joint senior authors.

Electronic supplementary material The online version of this article (https://doi.org/10.1007/s11095-019-2602-y) contains supplementary material, which is available to authorized users.

✉ Jill M. Steinbach-Rankins
jmstei01@louisville.edu

1 Department of Bioengineering, University of Louisville
505 S. Hancock, CTR 623, Louisville, Kentucky 40202, USA

2 Department of Biology, University of Louisville
Louisville, Kentucky, USA

3 School of Medicine, University of Louisville
Louisville, Kentucky, USA

4 James Graham Brown Cancer Center, University of Louisville
Louisville, Kentucky, USA

5 Department of Pharmacology and Toxicology, University of Louisville
Louisville, Kentucky, USA

6 Department of Microbiology and Immunology, University of Louisville
Louisville, Kentucky, USA

7 Center for Predictive Medicine, University of Louisville
Louisville, Kentucky, USA

ABBREVIATIONS

AUC	Area under the curve
C6	Coumarin 6
CPP	Cell penetrating peptide
DCM	Methylene chloride
diH2O	Deionized water
Dox	Doxorubicin
EPR	Enhanced permeability and retention
FRT	Female reproductive tract
HPV	Human papilloma virus
MDR	Multi-drug resistant
MEM	Minimum essential media
MFI	Mean fluorescence intensity
NaDC	Sodium deoxycholate
NP	Nanoparticle
o/w	Oil-in-water
PA-NHS	Palmitic acid-N-hydroxysuccinimide ester

PBS	Phosphate buffered saline
PEG	Polyethylene glycol
Pgp	P-glycoprotein
PLGA	Poly(lactic-co-glycolic) acid
PVA	Polyvinyl alcohol
RPMI	Roswell Park Memorial Institute medium
SEM	Scanning electron microscopy

INTRODUCTION

Chemotherapy for cervical cancer has had marginal success due to the lack of specificity attained with systemic administration, resulting in higher doses to achieve efficacy, increased adverse effects, rapid active agent clearance, and the emergence of chemotherapeutic resistance. Localized delivery can circumvent some of these challenges; however, delivery to the female reproductive tract (FRT) can result in rapid vaginal clearance, and thus difficulty maintaining efficacious drug concentrations. Yet even if administration is optimized, primary challenges for chemotherapy when treating tumor lesions with hypovascularized cores, such as typically occur with cervical cancer (1), are poor distribution and corresponding inefficacy, dependent on administration method and the tumor microenvironment (2,3). In particular, the cell origin or cervical cancer type has a significant role in the development and diversity of this microenvironment, resulting in different transport hurdles even for tumors of the same size and stage. Moreover, depending on cancer type, the degree of tumor cell density and intercellular junction formation have been shown to play key roles in the pharmacokinetics of chemotherapeutics within solid tumors (2,4–6).

To address these challenges, nanotherapeutic delivery vehicles have been designed to more safely and effectively promote active agent delivery directly to the tumor site, and to enhance agent distribution within the tumor microenvironment, with the end goal to promote penetration and subsequent uptake (7,8). Nanotherapeutic platforms, such as polymeric nanoparticles (NPs), provide a system in which encapsulation of chemotherapeutic agents can be achieved to prolong active agent stability and release, while limiting the drug exposure for healthy, surrounding tissue. Furthermore, NP accumulation in tumor tissue can be promoted via the enhanced permeability and retention (EPR) effect. FDA-approved polymer-based platforms such as poly(lactic-co-glycolic) acid (PLGA) NPs, have been engineered to reduce unwanted immunogenic responses, avoid organ clearance and tissue transport, target tumor tissue, penetrate the tumor interstitium, improve uptake, and enhance therapeutic efficacy (9,10). These platforms can also be tailored by altering the hydrophilic properties of the monomer subunits or polymer ratios to reduce the burst release of chemotherapeutics or other encapsulated agents. These modifications have the potential to provide sustained-delivery, corresponding with high uptake and antitumor effects, as has been shown in in a variety of cervical *in vitro* cultures and *in vivo* tumors (11).

The utilization of NP platforms to deliver chemotherapeutic agents has grown more prevalent in efforts to overcome the multi-drug resistant (MDR) properties of cervical cancers (12,13). Several studies have demonstrated enhanced efficacy of doxorubicin (Dox) by utilizing either inorganic or organic NP delivery systems (7,14). A recent study investigated the use of folic acid conjugated quantum dots to deliver Dox to folate receptor-positive cervical cancer cells, demonstrating significant improvement in cellular uptake and therapeutic efficacy (15). However, a separate study utilizing boron nitride NPs loaded with Dox, found that these NPs only offered a modest therapeutic effect in KB cervical cancer cells relative to leukemia cell lines (16). The differential results observed in these studies, highlight the effect that different delivery platforms can have in overcoming MDR in similar tumor types.

To better understand the effects of Dox and Dox-loaded NPs on cervical cancer cells with MDR, it was found that the use of Dox-conjugated NPs resulted in a high level of Dox within cells, relative to free Dox. Furthermore, murine studies that administered PLGA NPs that incorporated Dox and folic acid-polyethylene glycol surface modifications, demonstrated significantly increased efficacy, resulting in reduced tumor volume *in vivo*, relative to unmodified NPs and free Dox (17). These promising results suggest that the use of NP delivery platforms may increase the therapeutic efficacy of Dox and other drug candidates, particularly for MDR cervical cancers.

While these studies have helped to elucidate the attributes of Dox administration with NPs, NP penetration of the tumor interstitium and internalization by target cells remain primary issues that still challenge NP-mediated delivery and therapeutic efficacy of chemotherapeutics and other active agents. To overcome these transport-based challenges, NPs have been surface-modified with a variety of ligands to enhance tumor targeting and distribution.

Previously, we investigated the effects of NP surface-modification with cell-penetrating peptides (CPPs), stealth ligands, and tumor targeting ligands (MPG (unabbreviated notation), PEG (polyethylene glycol), and Vimentin, respectively), on NP penetration and distribution within the hypovascularized cervical tumor environment (18). More recently, we evaluated the penetration and distribution of MPG, PEG, and CPP-stealth (MPG/PEG) NP co-treatment strategies as a function of tumor size and morphology in 3D spheroid models of hypovascularized cervical cancer tissue (19). The differences in NP distribution as a function of surface modification (unmodified, MPG, PEG, or MPG/PEG co-treatment), spheroid morphology, and cervical cancer type, were assessed in HeLa, cervical epithelial adenocarcinoma cells; CaSki, cervical epidermoid carcinoma cells; and SiHa, grade II cervical squamous cell carcinoma cells, selected due to their MDR properties.

Building upon this previous work, the goal of this study was to determine the therapeutic efficacy imparted by these various delivery vehicles across these different cervical tumor types. Key differences include: CaSki cells form tight intercellular junctions (20), HeLa cells have an enhanced rate of aerobic glycolysis (21), and both SiHa and HeLa have lower levels of gap junction formation compared to CaSki cells (22). The chemotherapeutic agent, Dox, was incorporated into PLGA NPs with MPG or PEG modifications to assess the differences in efficacy imparted as a function of surface modification, NP co-treatment, transport, and cell type. The NP efficacy was assessed in 3D (spheroid) culture to create a system that more faithfully represents *in vivo* cervical tumors, typically having peripheral tissue hypervascularization and interior hypovascularization (1). The chemotherapeutic Dox was chosen due to its application in a variety of chemotherapeutic regimens, including cervical cancer, and its ability to affect tumor cells at any stage of the cell cycle (23,24). While Dox has proven efficacious in inhibiting both blood cancers and solid tumors, it is limited by the development of drug resistance, primarily caused by drug-resistant pumps such as P-glycoprotein (Pgp) – notably expressed in cervical cancer cells (7,12,13) – and an increase in intracellular antioxidant defense (25). Dox is also associated with acute side effects such as cardiomyopathy, due to non-specific targeting. These limitations offer opportunities for engineered delivery systems to improve upon its clinical efficacy.

MATERIALS AND METHODS

Nanoparticle Synthesis

Avidin-palmitate was synthesized for subsequent conjugation to NPs as previously described (18,19,26,27). Briefly, 40 mg of avidin (A9275, Sigma) was dissolved in 4.8 mL of 2% sodium deoxycholate (NaDC) in phosphate buffered saline (PBS) warmed to 37°C. Palmitic acid-NHS (PA-NHS, Sigma) was dissolved in 2% NaDC to a final concentration of 1 mg/mL and sonicated until well-mixed. PA-NHS solution (3.2 mL) was added dropwise to the avidin NaDC solution, and reacted overnight at 37°C. The following day, the reaction was dialyzed in 1200 mL of 0.15% NaDC in PBS heated to 37°C. Free PA-NHS was dialyzed overnight at 37°C using 3500 MWCO tubing to remove free palmitic acid. After overnight dialysis, the dialysis tubing contents were transferred to a storage vial and stored at 4°C until use.

PLGA NPs encapsulating either the fluorophore Coumarin 6 (C6) or the chemotherapeutic doxorubicin (Dox) were formulated as previously described (18,19,28) to enable visualization via fluorescence microscopy and induce cell death, respectively. It has previously been observed that negligible quantities of C6 are released (29–31). Briefly, NPs were formulated using an oil-in-water (o/w) single emulsion technique (18,19,27,28). Carboxyl-terminated poly(lactic co-glycolic acid, PLGA) (0.55–0.75 dL/g, LACTEL®) was used to synthesize 100–200 mg batches. Encapsulant was dissolved in methylene chloride (DCM) overnight at a concentration of 15 μg C6 per mg of PLGA or 100 μg Dox per mg PLGA. The following day, the PLGA/encapsulant/DCM solution was added dropwise to a 5% polyvinyl alcohol (PVA) solution of equal volume, vortexed, and sonicated. The resulting NPs were hardened in 0.3% PVA during solvent evaporation for 3 h.

Unmodified NPs were washed after hardening, and centrifuged at 4°C, 3 times in deionized water (diH_2O) to remove residual solvent. Nanoparticles were frozen, lyophilized, and stored at −20°C until use. A similar protocol was followed to synthesize MPG (3177 Da, GenScript) and PEG (5000 Da, Nanocs Inc.) surface-modified NPs, with the addition of avidin-palmitate (5 mg/mL) to the 5% PVA solution. Surface-modified NPs were collected after the first wash, and incubated for 30 min. with biotinylated ligands at a molar ratio of 3:1 ligand:avidin in PBS. After the ligand binding reaction, the NPs were washed two more times with diH_2O centrifugation, frozen, and lyophilized. All NPs were stored at −20°C after synthesis.

Nanoparticle Characterization

NP Physical Properties

NP characterization confirmed the physical NP properties including unhydrated diameter, morphology, and surface charge. Scanning electron microscopy (SEM, Zeiss SUPRA 35VP) was utilized to verify unhydrated NP morphologies and diameters, measured using NIH ImageJ software. The NP zeta potentials were characterized using a Malvern Zetasizer (Zetasizer Nano ZS90).

Loading and Release

To evaluate loading and encapsulation efficiency, approximately 3–5 mg of Dox NPs were suspended in 1 mL of DMSO for 30 min to dissolve the PLGA polymer matrix. Subsequently, the quantity of Dox loaded was determined by centrifuging the Dox NP/DMSO suspension to remove NPs, followed by measuring the fluorescence (480 nm) of the supernatant, and comparing to a calibrated Dox standard. The sustained-release properties of Dox NPs were determined by assessing controlled release *in vitro*. Dox NPs were resuspended in 1 mL of 1X PBS (pH 7.4) at a concentration of 2 mg/mL and incubated with gentle agitation at 37°C. At fixed time points (1, 2, 4, 6, 24, 48, 72, 96 h, 1, 2, 3, and 4 wk), samples were collected and the amount of Dox released

from the NPs was quantified using absorbance (480 nm) as described above.

Tumor Spheroid Cell Culture

The human cervical carcinoma cell lines, SiHa, and CaSki (ATCC), were kindly provided by Dr. Alfred Jenson (University of Louisville), while the HeLa cell line was generously provided by Dr. Kenneth Palmer (University of Louisville). HeLa and SiHa cells were maintained in Minimum Essential Media (MEM) and CaSki cells were maintained in Roswell Park Memorial Institute Medium (RPMI) medium, both supplemented with 10% fetal bovine serum and 1% penicillin-streptomycin. All cells were kept in a humidified atmosphere of 5% CO_2 at 37°C, and were grown to 80% confluence prior to tumor spheroid formation.

Hanging Drop Tumor Spheroid Formation

To form hanging drop spheroids, ultra-low attachment plates (#4515, Corning) were utilized. Briefly, cells were trypsinized after reaching 80–90% confluency and seeded at a density of 5000 cells per well in 100 μL culture medium. Care was taken to minimize pipette tip contact with ultra-low attachment plate well walls. Spheroids were allowed to form for 5 days under the cell culture conditions described above.

Spheroid Characterization

Spheroid morphology was characterized prior to NP administration. Briefly, spheroids were removed from culture plates and placed on imaging dishes (P35G-0-14-C, MatTek) in 25 μL of culture medium to prevent drying. Spheroids were then imaged with an epifluorescent microscope (Axiovision 4, Zeiss) under transmitted light using a 10X objective.

Flow Cytometry

The association and internalization of NPs were determined using fluorescence-activated cell sorting (FACS). The four NP formulations: unmodified, MPG, PEG, and MPG/PEG co-treatment groups, were added to hanging drop spheroids for 1.5 or 24 h. After incubation, the spheroids were collected in 2 mL eppendorf tubes and washed three times with PBS to remove unbound NPs. Trypsin-EDTA (0.25%) was added to the spheroids for 5 min to dissociate the spheroids. Trypsinized cells were subsequently moved to FACS tubes, centrifuged, and resuspended in a FACS buffer solution containing 1% BSA and 0.1% sodium azide. To assess total cell association (NP bound to and internalized), half the cells from each sample were moved to separate FACS tubes and kept on ice until analyzed. To assess cellular internalization, the remaining cells were exposed to 0.4% trypan blue for 5 min to quench extracellular fluorescence, washed twice in FACS buffer, and kept on ice until analyzed. All FACS tubes from both groups were analyzed using a BD LSRFortessa Flow Cytometer (BD Biosciences). Data were analyzed using FlowJo software (FlowJo Enterprise), and a minimum of 2500 cells were analyzed per sample.

NP Efficacy in Cervical Cancer Cell Line Tissue Culture

Efficacy in Monolayer Culture

The efficacy of surface-modified Dox NPs in monolayer cell cultures was determined via the MTT (3-(4, 5-dimethylthiazolyl-2)-2, 5-diphenyltetrazolium bromide) cell proliferation assay (ThermoFisher Scientific). Cervical carcinoma cells were seeded at a density of 1.5×10^3 cells per well and allowed to adhere overnight. Serial dilutions of surface-modified Dox NPs at a maximum NP concentration of 5 mg/mL, were administered to cell monolayers. Untreated cells and cells treated with 10% DMSO were used as positive and negative controls of viability, respectively. Cells were then incubated under normal cell culture conditions for 24 h. Following NP administration, media was discarded and replaced with 100 μL of fresh PBS. Plates were then centrifuged at 471 x g (300 rpm) for 5 min, to remove free NPs. The PBS supernatant was discarded from the wells, and 10 μL MTT reagent was added to each well in the absence of light. Plates were subsequently incubated under normal cell culture conditions for 4 h. Following incubation, 50 μL lysis buffer (10% SDS in 0. 01 M HCl) was added to each well and placed in the incubator overnight. Sample absorbance was quantified (570 nm) the next day.

Efficacy in 3D Spheroid Cell Culture

To assess NP efficacy in tumor spheroids, four different NP formulations were evaluated: unmodified, MPG, PEG, and MPG/PEG co-treatment groups. Once spheroid formation was achieved using the hanging drop method (5 days), fresh culture medium was added and the spheroids were transferred to 96-well opaque plates with 100 μL media and NP treatments for 24 h. For the NP co-treatment group, a half-dose of the MPG and PEG NPs were combined for a total NP dose of the desired concentration. After 24 h, the plated spheroids were removed from the incubator and equilibrated for 30 min. Cell Titre-Glo (100 μL) was added to each well, and the plate contents were mixed vigorously for 5 min on a reciprocating shaker. After mixing, the spheroids were incubated at room temperature for 25 min and luminescence was recorded on a BioTek Synergy HT luminometer.

Statistical Analysis

A minimum of 6 biological replicates were used to collect NP efficacy data for both 2D and 3D cell cultures, and 3 technical repeats were conducted for flow cytometry data acquisition. All statistical significance was determined using a one-way ANOVA post-hoc Tukey test, $p < 0.05$.

RESULTS

Nanoparticle Characterization

NP Physical Properties

NP size and morphology were confirmed using SEM and ImageJ software. Unhydrated NPs demonstrated a spherical morphology, with diameters ranging between 160 to 180 nm (18,19). Hydrated NP diameters (18) and surface charges were measured using a Zetasizer (Malvern Zetasizer Nano ZS90). Unmodified NPs had a negative surface charge of -14.8 ± 1.2 mV; while MPG- and PEG-modified NPs measured 0.7 ± 0.3 and 0.1 ± 0.4 mV, respectively, validating surface ligand conjugation. The degree of ligand substitution was previously characterized in (26).

Loading and Release

Doxorubicin loading and encapsulation efficiency within MPG, PEG, and unmodified NPs were assessed (Table I). MPG and PEG NPs exhibited significant increases in drug loading (65.9 ± 2.3 μg/mg and 75.7 ± 6.8 μg/mg) and encapsulation efficiency (66% and 76%), relative to unmodified NPs (28.9 ± 1.5 μg/mg and 29% respectively). The *in vitro* release of Dox was characterized during a 24 h release study (Fig. 1). The unmodified NPs released approximately 95% of the encapsulated Dox during the first 24 h, while MPG and PEG NPs released ~80–90% during the same duration.

Spheroid Morphology and Nanoparticle Association

Tumor spheroids were formed from each HeLa, SiHa, and CaSki cervical cell lines. Spheroid morphology was found to be dependent upon cervical cancer type (Fig. 2), as previously observed (19), and is hypothesized to impact NP therapeutic efficacy. Overall, HeLa cells demonstrated the most diffuse morphology, while CaSki cells formed the most dense tumor spheroids.

To assess differences in NP localization as a function of spheroid morphology (Fig. 2), NP association and internalization were evaluated following incubation times of 1.5 and 24 h (Fig. 3). Differences in association (NPs bound plus internalized), relative to internalization, varied as a function of both incubation time and cancer cell type. The association and internalization were similar for each cell type 1.5 and 24 h post-administration, indicating that equilibrium was reached early.

Within HeLa spheroids, MPG NPs exhibited a statistically significant increase in cellular association after 24 h administration, relative to unmodified and PEG NPs. Co-treatment NPs (MPG/PEG) had no statistical difference relative to the other NP groups. Furthermore, no statistically significant differences were observed in internalization amongst the NP treatment groups.

In the similarly sized, but less amorphous SiHa spheroids, all the NP groups had statistically similar association. Moreover, all surface-modified NP groups had statistically similar cellular internalization. However, NP internalization was generally higher in SiHa spheroids than for the other cell types.

In the smaller, densely structured CaSki spheroids, NP association was lower after 24 h across all treatment groups compared to that in HeLa and SiHa spheroids. MPG/PEG co-treatment NPs had increased cellular association with respect to the other NP groups, which were statistically similar. All NP groups had comparable internalization, with statistical differences only observed between MPG/PEG co-treatment and PEG NPs. Overall, NP internalization was of the same magnitude as observed in the HeLa cells, while the surface-modified NPs, demonstrated lower internalization than seen in SiHa cells. The association was also generally lower than observed in the other cell types.

Table I Nanoparticle Loading and Encapsulation Efficiency

NP Formulation	Concentration (μg Dox per mg NP)	Encapsulation
MPG	65.9 ± 2.3	66%
PEG	75.7 ± 6.8	76%
Unmodified	28.9 ± 1.5	29%

Nanoparticle-Mediated Drug Cytotoxicity

To assess the impact of NP transport on chemotherapeutic efficacy, surface-modified NPs were administered to cervical cancer spheroids (Fig. 5 **and Supp.** Fig. 2), and compared to that in cell monolayers (Fig. 4 **and Supp.** Fig. 1) representing an optimal exposure condition (such as for tumor cells next to the vascular supply *in vivo*). The concentration at which 50% of cell growth was inhibited (IC50) was evaluated for each NP treatment group as a function of Dox concentration (Figs. 4 and 5**,** Table II) and NP dose (**Supp.** Figs. 1 and 2**, Supp. Table I)**. The efficacy imparted by NPs was found to vary as a function of cervical tumor and NP modification type. Figure 6 summarizes the IC50 values as a function of Dox and NP

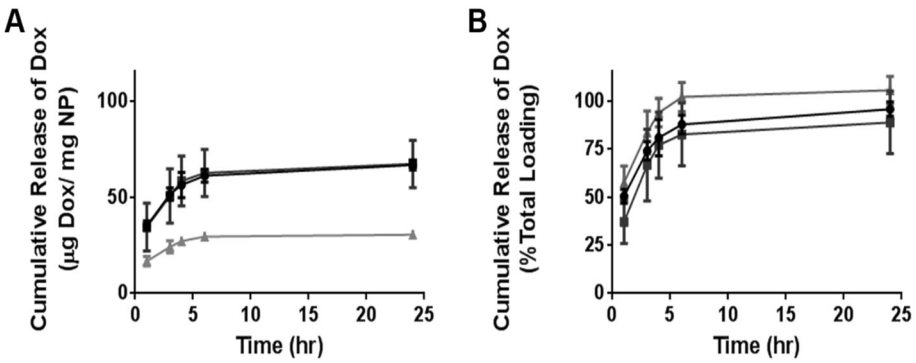

Fig. 1 Cumulative release of Dox from unmodified (triangle), MPG (circle), and PEG (square) modified NPs, as a function of (**a**) NP mass and (**b**) percent total loading.

concentrations. Last, we assessed how the NP distribution in the 3D cell cultures of the various cell types, as observed in our previous work (19), related to their chemotherapeutic efficacy measured in this study (Table III).

NP Efficacy in HeLa Cells

In HeLa spheroids, the MPG/PEG co-treatment NP group demonstrated a significant increase in efficacy (IC50 13.3 ± 0.64 μM, Fig. 6 and Table II) relative to other NP groups. Free doxorubicin evinced statistically similar efficacy to the MPG/PEG co-treatment.

In HeLa monolayers, unmodified NPs demonstrated the greatest efficacy, with a significant decrease in IC50 (20.3 ± 2.2 μM) relative to MPG (28.6 μM),PEG (39.5 μM), and free Dox (25.4 ± 3.9 μM). In monolayers, only unmodified NPs were more efficacious than free Dox.

NP Efficacy in SiHa Cells

Relative to their modest efficacy in HeLa spheroids, unmodified NPs exhibited the greatest efficacy relative to other surface-modified NP groups in SiHa spheroids. Unmodified NPs exhibited a statistically lower IC50 (14.7 ± 0.6), relative to MPG (30.2 ± 1.2), PEG (23.3 ± 1.1 μM), and the MPG/PEG co-treatment NPs (28.4 ± 4.2 μM). There were no differences in efficacy observed between MPG, PEG, and MPG/PEG co-treatment NPs. Overall, all NP groups provided modest efficacy in SiHa spheroids, while only unmodified NPs provided comparable efficacy to free Dox. Similar to HeLa spheroids, free Dox exhibited the lowest IC50 (11.9 ± 2.9 μM), with statistical significance observed relative to all surface-modified NP groups.

In SiHa monolayers, PEG and MPG/PEG co-treatment NP groups exhibited the strongest efficacy (IC50s 22.6 ± 3.9 μM and 27.2 ± 3.3 μM) with improved efficacy relative to free Dox (IC50 42.3 ± 13.7 μM). However, no statistical differences were observed across NP formulations, with respect to each other. While unmodified NPs showed the greatest efficacy in SiHa spheroids, PEG and MPG/PEG co-treatment NPs performed most efficaciously, relative to free Dox, in the monolayers.

NP Efficacy in CaSki Cells

PEG NPs were the most efficacious treatment group in CaSki spheroids (IC50 13.1 ± 1.1 μM), demonstrating a significant improvement in efficacy relative to all other treatment groups. No statistical differences were observed between unmodified, MPG, and MPG/PEG co-treatment NPs. As in HeLa and SiHa spheroids, free Dox exhibited the lowest IC50 (1.8 ± 0.5 μM), relative to all NP groups.

For CaSki monolayers, all NP groups, except MPG, demonstrated significant improvements in efficacy, relative to free Dox. Within the NP groups, MPG/PEG co-treatment NPs were more efficacious than MPG NPs (IC50s 18.1 ± 2.3 and 31.3 ± 5.4 μM), but demonstrated similar efficacy to PEG and unmodified NPs.

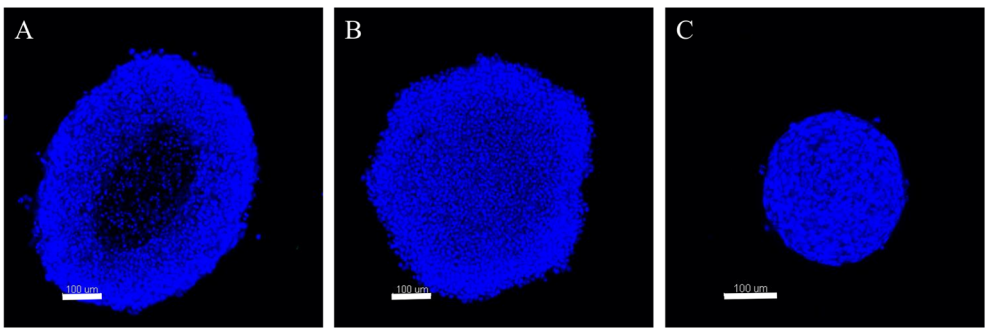

Fig. 2 Fluorescent cross-sectional images of cervical tumor spheroids comprised of (**a**) HeLa, (**b**) SiHa, and (**c**) CaSki cervical cancer cells stained with Hoechst dye. Scale bar represents 100 μm.

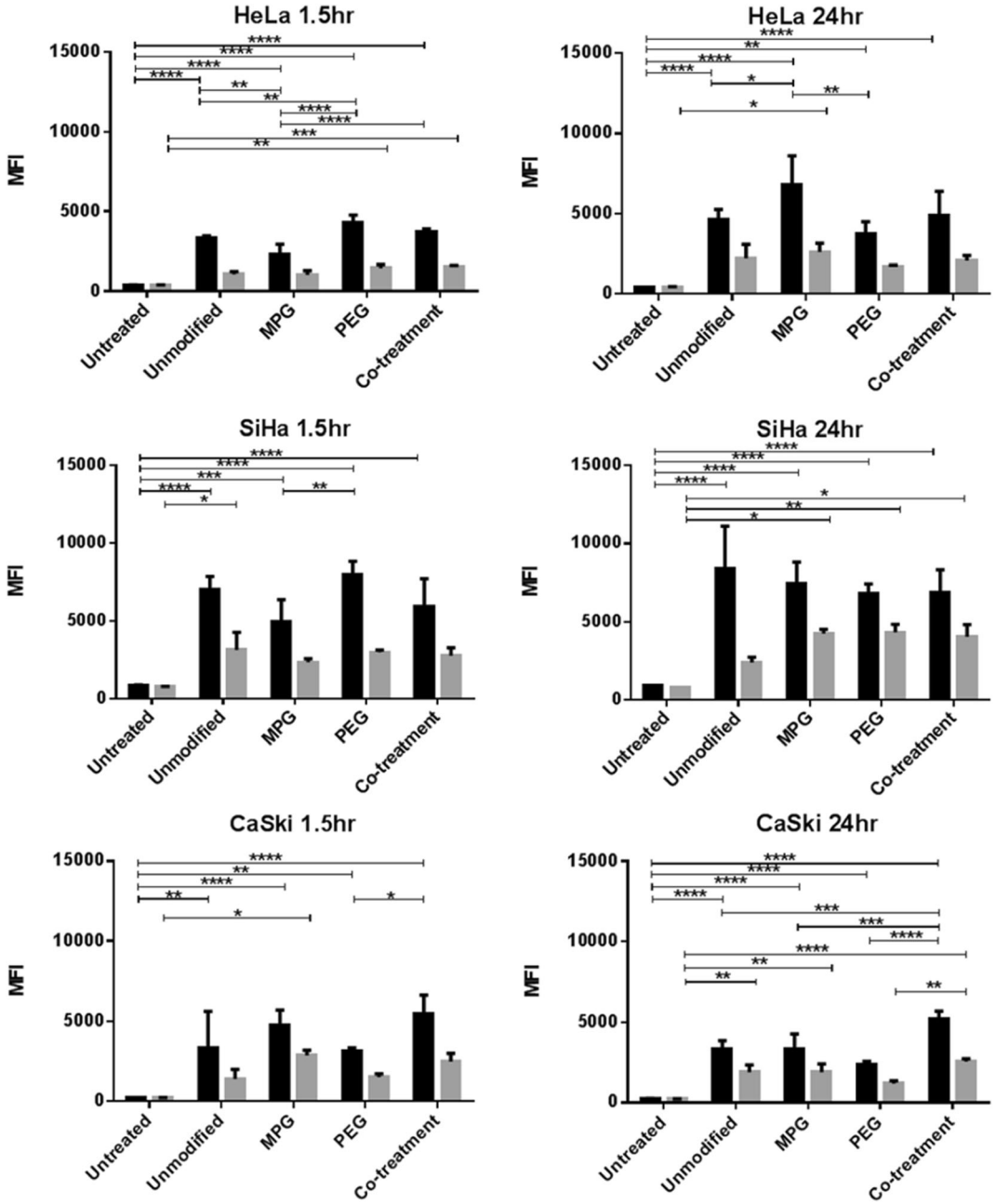

Fig. 3 NP association (binding plus internalization, black) and internalization (grey) in cervical cell line spheroids after 1.5 h (left) and 24 h (right) administration. Asterisks denote a statistically significant difference between two groups (* $p < 0.01$, ** $p < 0.001$, *** $p < 0.0001$, **** $p < 0.00001$).

DISCUSSION

The effect of surface modification on NP penetration and cell internalization in cervical tumor tissue was recently investigated (18). In both HeLa monolayers and spheroids, nanoparticles modified with the CPP MPG exhibited the highest cellular internalization. However, internalization primarily occurred within the spheroid periphery, resulting in a modest (< 100 μm) tumor penetration depth. In contrast, PEG-modified NPs distributed most deeply into spheroids, but were less readily internalized by cells, underscoring the dichotomous transport properties of NPs modified with a CPP, relative to a neutral "stealth" ligand.

We subsequently evaluated surface-modified NP distribution as a function of cervical tumor type and morphology, in addition to NP surface-modification (19). In small, homogeneously shaped avascular tumors, enhanced distribution was observed for MPG and PEG NPs in HeLa, and for all surface-modified NPs in SiHa spheroids, relative to unmodified NPs. In larger, more irregularly-shaped spheroids, the greatest distribution was observed for MPG and MPG/PEG co-treatment NPs in HeLa, and for PEG and MPG/PEG

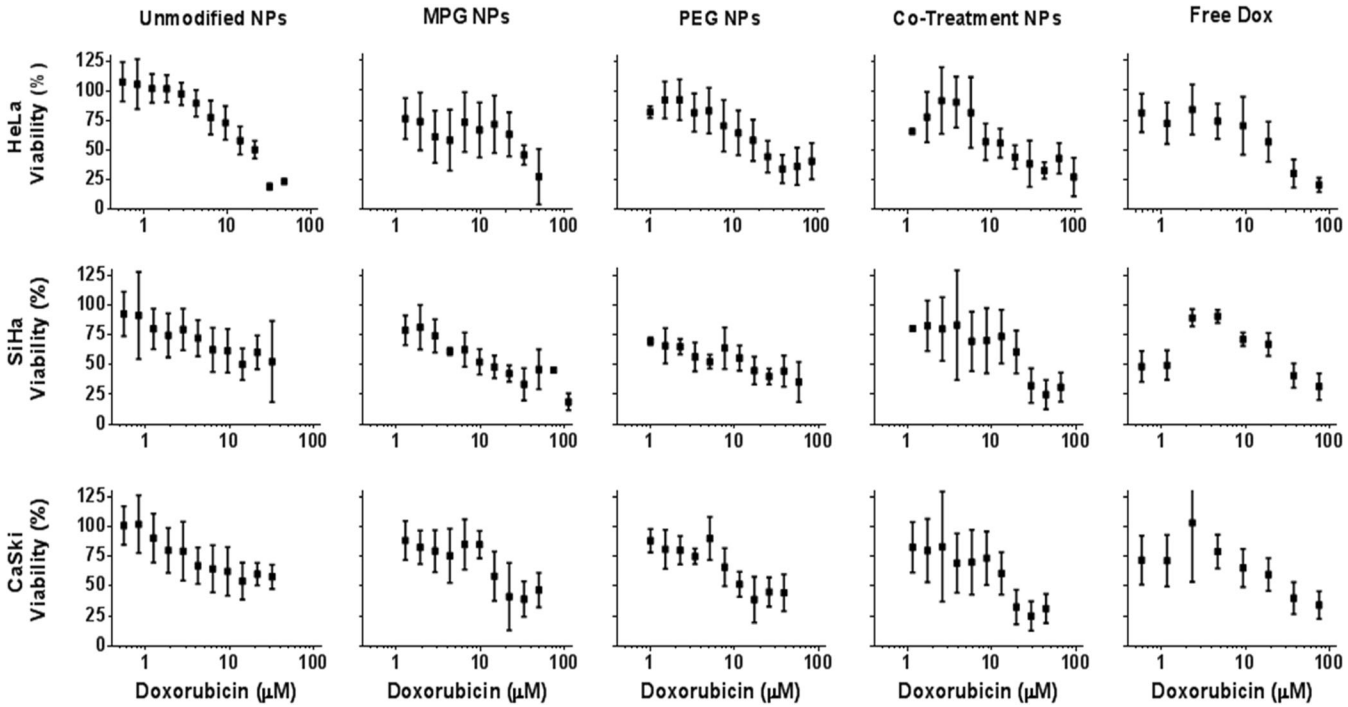

Fig. 4 Cytotoxicity of surface-modified Dox NPs and free Dox in HeLa, SiHa, and CaSki cervical carcinoma monolayers after 24 h administration, as a function of Dox dose.

co-treatment NPs in SiHa spheroids (19). In contrast, small, densely structured CaSki spheroids exhibited modest distribution across all NP groups. The variation in spheroid morphology across cell types (Fig. 2) was observed to significantly impact NP penetration and distribution (19). Overall, for a given tumor type, surface modifications were found to benefit tumor distribution, relative to utilization of unmodified NPs. These results suggested that co-treatment strategies may overcome the obstacles associated with NP tumor penetration and distribution, and may influence the design of

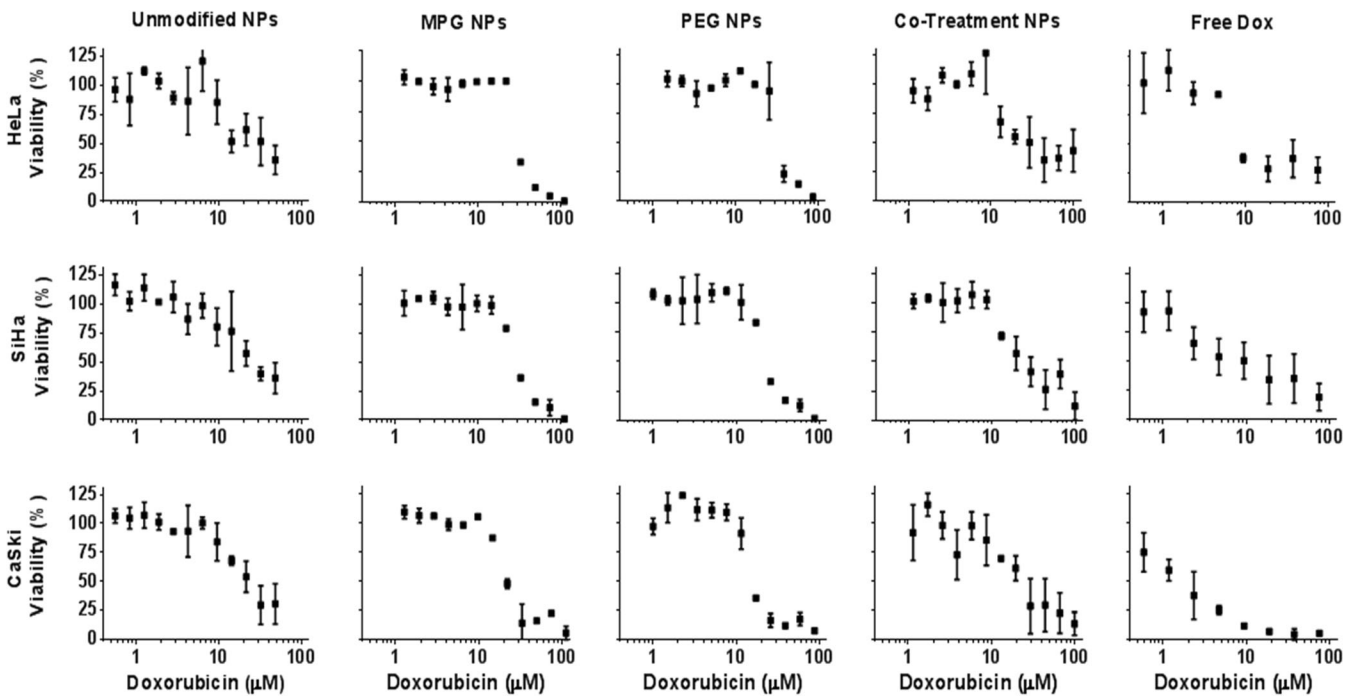

Fig. 5 Cytotoxicity of surface-modified Dox NPs and free Dox in HeLa, SiHa, and CaSki cervical carcinoma cell line spheroids after 24 h administration, as a function of Dox dose.

Table II IC50 Values of Surface-Modified Dox NPs and Free Dox in Cervical Cancer Cell Line Monolayers and Spheroids, Expressed in Terms of Dox Concentration

Cervical cancer cell model		Doxorubicin IC50 [μM]				
		Free Dox	Unmodified NPs	MPG NPs	PEG NPs	Co-Treatment NPs
Monolayers	HeLa	25.4 ± 3.9	20.3 ± 2.2	28.6 ± 4.0	39.5 ± 7.5	35.8 ± 8.6
	SiHa	42.3 ± 13.7	27.7 ± 5.8	34.1 ± 8.5	22.6 ± 3.9	27.2 ± 3.3
	CaSki	41.4 ± 10.5	29.7 ± 7.9	31.3 ± 5.4	23.4 ± 4.5	18.1 ± 2.3
Spheroids	HeLa	8.7 ± 1.3	33.4 ± 5.5	31.9 ± 6.5	34.7 ± 1.6	13.3 ± 0.6
	SiHa	11.9 ± 2.9	14.7 ± 0.6	30.2 ± 1.2	23.3 ± 1.1	28.4 ± 4.2
	CaSki	1.8 ± 0.5	25.38 ± 2.6	22.5 ± 3.2	13.1 ± 1.1	25.6 ± 3.7

delivery platforms for cancer therapy, especially for tumors expected to present both regularly- and irregularly-shaped tissue regions.

Given these previous observations, the aim of this study was to relate the transport properties of surface-modified NPs (18,19) to therapeutic efficacy as a function of cervical cancer type. To evaluate this, the efficacy of unmodified and surface-modified NPs, encapsulating the chemotherapeutic Dox, was assessed in three cervical carcinoma cell lines (HeLa, SiHa, and CaSki), grown as 3D spheroids to represent tumor lesions with a hypervascularized periphery and hypovascularized interior. We selected Dox, as it is a commonly used chemotherapeutic; however, its efficacy against cervical tumors has been limited due to the MDR of several cervical cancer types, including HeLa, SiHa, and CaSki lines. We hypothesized that the use of NPs may significantly increase the therapeutic efficacy of Dox, by increasing intracellular Dox accumulation, as MDR cells are prone to have more drug efflux due to an increased presence of P-glycoprotein pumps (7,32–34). Moreover, the mechanism of action of Dox intercalation with DNA, inducing topoisomerase II inhibition and cellular DNA damage, makes it a model drug to represent active agents that must internalize to elicit therapeutic effect.

While the purpose of this study was to assess the effect of NP surface-functionalization on cervical tumor cytotoxicity, drug loading and release have integral roles in achieving therapeutic effect. The modest encapsulation efficiencies of unmodified NPs (29%), relative to MPG- and PEG-modified NPs (66 and 76% of Dox, respectively, Table I), resulted in variations of release quantity with respect to time. Unmodified

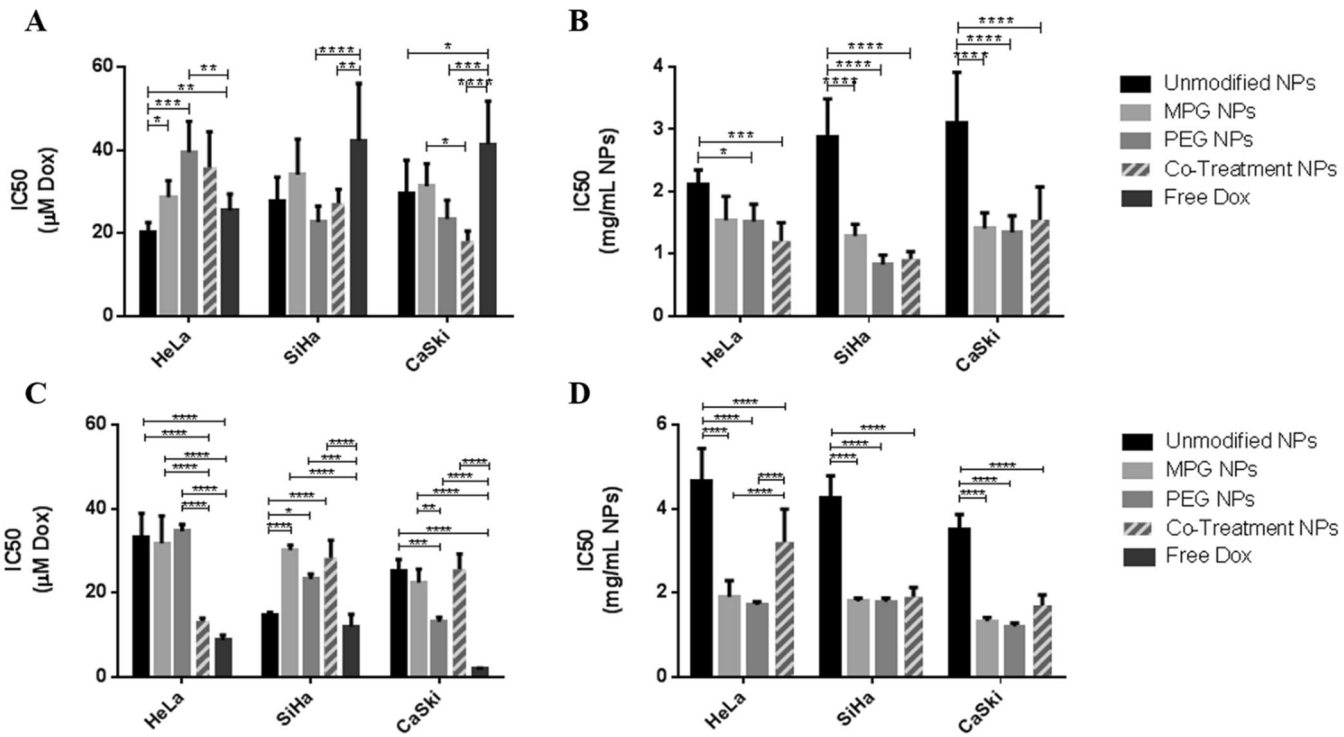

Fig. 6 IC50s of surface-modified NPs after 24 h administration in cervical carcinoma cell line monolayers (top) and spheroids (bottom) as a function of Dox (A and C, μM) and NP (B and D, mg/mL) concentrations. Asterisks denote a statistically significant difference between two groups (* $p < 0.01$, ** $p < 0.001$, *** $p < 0.0001$, **** $p < 0.00001$).

Table III Comparison of NP Efficacy (Measured as IC50 in this Study) to NP Distribution (Quantified as Area-Under-the-Curve, AUC (MFI-μm), in (19)) and Maximum Penetration (Measured as Mean Fluorescence Intensity (MFI) as a Function of Maximum Penetration Depth (μm), in (19)) in 3D Cell Culture of Various Cervical Cancer Cell Types

NP measurement	Cell type	Unmodified	MPG	PEG	Co-treatment
Efficacy shown as IC50 (μM)	HeLa	33.4 ± 5.5	31.9 ± 6.5	34.7 ± 1.6	13.3 ± 0.6
	SiHa	14.7 ± 0.6	30.2 ± 1.2	23.3 ± 1.1	28.4 ± 4.2
	CaSki	25.4 ± 2.6	22.5 ± 3.2	13.1 ± 1.1	25.6 ± 3.7
Distribution shown as AUC (MFI-μm)	HeLa	15,841 ± 1637	47,018 ± 8754	23,140 ± 5531	15,657 ± 3579
	SiHa	14,673 ± 543	24,972 ± 2020	24,237 ± 2532	26,970 ± 5574
	CaSki	9331 ± 1090	12,364 ± 1485	14,297 ± 281	11,847 ± 2231
Fluorescence Observed at Max. Penetration Depth (MFI, μm)	HeLa	(99, 85)	(225, 129)	(217, 82)	(154, 102)
	SiHa	(123, 61)	(222, 91)	(135, 64)	(239, 84)
	CaSki	(83, 52)	(101, 66)	(238, 78)	(84, 90)

NPs released 28.3 ± 2.1 μg Dox/mg NP within 24 h, while MPG and PEG NPs exhibited significantly higher release (66.5 ± 2.6 and 67.2 ± 12 μg Dox/mg NP, respectively) during the same duration (Fig. 1). The decreased loading, seen in unmodified NP formulations, may be partially due to increased amounts of Dox diffusing from unmodified, relative to surface-modified NPs, during the fabrication process.

When compared as a function of Dox concentration, relative to NP dose, these loading and release differences had an impact on therapeutic efficacy (measured as the IC50). For example, unmodified NPs, which were the most efficacious in SiHa spheroids (14.7 ± 0.6 μM, Fig. 6**,** Table II) as a function of Dox concentration, required a higher NP dose (3–5 mg/mL, **Supp.** Table I), relative to surface-modified NPs, to achieve efficacy across all tumor types (HeLa, SiHa, CaSki). Furthermore, although they demonstrated modest efficacy relative to other NP treatment groups, unmodified NPs were still more efficacious than free Dox in CaSki and HeLa monolayers. Therefore, discrepancies in therapeutic efficacy as a function of NP dose relative to Dox dose, may be attributed to the approximately 2-fold lower drug loading and corresponding lower release observed with unmodified NPs. Moreover, as surface-modified NPs may release less encapsulant during the fabrication process, contributing to overall higher loading post-fabrication, these observations confirm the need to quantify therapeutic efficacy as a function of both drug release and NP dosing.

In addition to cytotoxicity differences based on NP loading and release profiles, the therapeutic efficacy of surface-modified NPs varied as function of cell type and NP surface modification. While unmodified NPs were most efficacious in SiHa spheroids as a function of Dox concentration, MPG/PEG co-treatment and PEG NPs were the most efficacious groups in HeLa and CaSki spheroids, respectively. Notably, in the more densely packed CaSki spheroids, PEG NPs were the most efficacious; however, all NP groups were less efficacious than free Dox. These results suggest that specific surface modifications, dependent on tumor type, may elicit similar therapeutic effect as free drug. These results are consistent with the fact that tumor cell type and the associated microenvironment significantly impact therapeutic efficacy.

Along with tumor microenvironment effects, active agent interaction with the tumor microenvironment has been explored to understand poor efficacy. Previous work investigated the effect of free Dox in tumor spheroids, and found that HeLa spheroids retained morphology and proliferated, even after treatment with a range of Dox concentrations (0–40 μM) (35). One proposed reason was that the extracellular matrix within the spheroid microenvironment remains intact following cell death (35). Specifically for Dox, it was observed that efficacious levels of Dox failed to be internalized within 24 h, resulting in reduced cytotoxic effect. Considering this, the use of specific NP modifications, while providing similar or less efficaciousness dependent on tumor type, may offer benefit within the real tumor microenvironment, by minimizing drug toxicity to surrounding tissue, providing longer exposure, and enhancing distribution. Moreover, NP diffusion, relative to free Dox delivery, may promote NP immobilization in the tumor matrix, prolonging the effects of localized cell death while reducing overall systemic cytotoxicity.

The effect of tumor density has also been determined to play a role in the pharmacokinetics of chemotherapeutics within solid tumors. In particular, tumors that have a reduced tissue density have increased molecule penetration (2,4–6). Similarly, in our previous studies, we observed that the decreased density of HeLa and SiHa spheroids, relative to CaSki spheroids correlated to increased levels of NP penetration (19). Additionally, the difference in levels of HPV genome incorporation and oncogenic E6/E7 expression between cervical tumor cells underscores the variations in spheroid growth and permeability as a function of cell type (36,37). In studies in (21) it was found that the expression of rate-limiting glycolytic enzymes was significantly influenced by incorporation of HPV oncogenes E6/E7, leading to enhanced rates of aerobic

glycolysis (21). The investigation revealed that the presence of these enzymes was dramatically elevated in HeLa cells, relative to CaSki and SiHa. This propensity for HeLa cells to have enhanced rates of aerobic glycolysis could significantly impact the gradient of proliferating cells in the tumor microenvironment. Another study by the same group found that under hypoxic conditions, HPV-positive cells can undergo a reversible state of dormancy and avoid senescence (38). This effect could also contribute to variations in regions of proliferating *versus* dormant cells, and impact the microenvironment at regions of gradient transition within the tissue.

In addition to the effects observed from oncogenic expression, other work has evaluated the role of gap junction formation in cervical cancer progression. These studies revealed that both HeLa and SiHa cells have negligible levels of Connexin 43 relative to CaSki cells, and therefore exhibit lower levels of gap junction formation (22). This is in agreement with our current and previous work, in which we observed that CaSki cells consistently formed compact, dense spheroids that are less permissive to NP transport (19). The dependency of pharmacokinetics on tumor spheroid intercellular interactions and cell density may also contribute to the increase in efficacy of MPG/PEG co-treatment NPs in HeLa spheroids relative to SiHa and CaSki spheroids. The more permeable nature of HeLa spheroids may be favorable for both MPG and PEG surface-modified NPs to more easily diffuse through the tissue. Alternatively, as in our previous work (18,19), the different distribution profiles of MPG and PEG NPs, may benefit from co-administration strategies (here, MPG/PEG co-treatment) that target tumor cells in different tumor regions (MPG: periphery, PEG: core). In contrast, the increased efficacy of unmodified NPs in SiHa spheroids and PEG NPs in CaSki spheroids, relative to the co-treatment in the less amorphous spheroids, suggests the advantage that modification may offer in enabling the delivery of therapeutically effective levels of active agent in tumors of increasing variability and unique microenvironment conditions.

Another aspect of NP efficacy that is often overlooked, is the relationship between transport and NP association and internalization at the target site. Thus, increased NP distribution and penetration into tumor tissue may not necessarily correlate with improved efficacy (Table III). While it has been previously established that Dox must be internalized to exert therapeutic effect, NPs contribute an additional layer of complexity (yet potential enhancement) to the delivery process. To relate these properties, we assessed total NP association (binding and internalization) and internalization dependent on cell and surface-modification type.

In HeLa spheroids, MPG NPs had the highest levels of cell association (bound extracellularly as well as internalized, 6823 MFI) relative to all other NP groups after 24 h administration, with statistical significance observed relative to unmodified and PEG NPs (Fig. 3). Although there was no statistical difference between NP groups for cell internalization (Fig. 3), the association results suggest that MPG NPs may be interacting with the extracellular components of the tumor periphery where proliferating cells are present, while PEG NPs encounter fewer interactions with the tumor microenvironment and diffuse more freely through the spheroid. This transport behavior, observed also in our previous work (19), may support the increase in efficacy of the MPG/PEG co-treatment NPs observed, particularly in more amorphously-shaped HeLa spheroids.

In SiHa spheroids, there were no statistical differences between NP groups for cell association after 24 h. (Fig. 3). Similarly, while all surface-modified NPs exhibited trends of improved cell internalization in SiHa spheroids relative to unmodified NPs, no statistical significance was observed (Fig. 3). Here, we hypothesize that even slight increases in cell association, seen with unmodified NPs, may correlate with the increase in therapeutic efficacy of unmodified NPs, relative to surface-modified NPs in SiHa spheroids. These results support the idea that tumor distribution must be considered to effectively deliver therapeutic levels of drug within the tumor microenvironment.

In CaSki spheroids, the MPG/PEG co-treatment group demonstrated higher cell association relative to all other NP groups and higher levels of cell internalization relative to PEG NPs (Fig. 3). Interestingly, the MPG/PEG co-treatment group was the most efficacious in CaSki monolayers (Figs. 4, 5 and 6, Table II) but the least efficacious NP group in CaSki spheroids. These results substantiate previously observed trends that the bulk of NP uptake occurs along the tumor periphery (for hypovascularized lesions) and for tissue proximal to the vasculature (for vascularized tumors). When delivering therapeutic agents, it is important to consider that an adequate amount of NPs and associated therapeutic payload may not be internalized in cells distal from the vascular supply. These results are consistent with our previous experimental (39–41) and computational modeling work (39,42–45).

While the effects of NP binding and penetration can be observed in tumor spheroids, the significance of NP penetration is even more pronounced for treatment in hypoxic tumor conditions, where hypoxia is often associated with elevated levels of chemoresistance (6). Our previous work (46–48) has confirmed that spheroid growth impacts cell proliferation, apoptosis, and necrotic/hypoxic core formation, consistent with previous studies (49). Moreover, these studies have noted that the outer layer (width ~100um) is mostly proliferative, the middle layer hypoxic, and the inner core necrotic. These microstructural differences, in which the inner tumor layer is comprised of hypoxic cells, may contribute to decreased cell sensitivity to Dox, as hypoxic cells would be quiescent and thus avoid damage by the drug action during the cell cycle. Also, transient hypoxia has been shown to activate and upregulate genes encoding P-glycoprotein and dihydrofolate reductase, leading to

resistance to drug substrates that are reliant on these molecules. In future, work, the impact of P-glycoprotein and other cellular factors affecting drug efficacy will be quantified by measuring these markers across different cancer types, with the goal to provide insight into how drug resistance may affect efficacy. Furthermore, tumor hypoxia has been shown to disrupt protein folding in the endoplasmic reticulum due to associated glucose deprivation (50–52). This protein misfolding induces drug resistance to topoisomerase II-targeted drugs, such as Dox. In addition, Dox is known to react in the presence of oxygen and reduce to a superoxide which contributes to cytotoxicity. Within the hypoxic regions of the tumor, these effects may be attenuated due to the decrease in free radical production. To overcome an increased drug resistance due to these phenomena, an effective delivery strategy would require NPs to adequately diffuse to tumor regions distal from the vasculature and undergo subsequent cell internalization. As the results here suggest, the ability of NPs to deliver an adequate therapeutic payload to inner tumor tissue is highly dependent on tumor cell type and NP surface modification. These results highlight the variability associated with treating cervical cancers of different disease origins, suggesting that an effective drug delivery strategy may be achieved by utilizing NP surface modification ligands tailored to the specific disease type. The observed changes in NP efficacy and transport provide insight into how NP delivery platforms can be designed and tailored for improved personalized treatment strategies against cancers with multiple disease etiologies.

CONCLUSION

This study utilizes both single and co-treatment surface-modified NP delivery strategies to assess the efficacy of the chemotherapeutic Dox against hypovascularized cervical tumors of different disease origins. The results highlight the dependency of therapeutic efficacy on tumor cell type and the associated microenvironment. Longer term, this offers the possibility to tailor NP-mediated delivery strategies to maximize therapeutic efficacy based on patient-specific tumor tissue characteristics.

ACKNOWLEDGMENTS AND DISCLOSURES

JSR acknowledges the Knight's Templar Foundation for providing partial funding to LBS and to the University of Louisville Cancer Education Program NIH/NCI R25-CA134283 for partial support of SP. The authors acknowledge partial support from NIH COBRE, grant number GM125504. The authors thank Dr. Sham Kakar (School of Medicine, University of Louisville) for the use of the Malvern instrument.

REFERENCES

1. Hockel S, Schlenger K, Vaupel P, Hockel M. Association between host tissue vascularity and the prognostically relevant tumor vascularity in human cervical cancer. Int J Oncol. 2001;19(4):827–32.
2. Au JL, Jang SH, Wientjes MG. Clinical aspects of drug delivery to tumors. J Control Release. 2002;78(1–3):81–95.
3. Cukierman E, Khan DR. The benefits and challenges associated with the use of drug delivery systems in cancer therapy. Biochem Pharmacol. 2010;80(5):762–70.
4. Grantab R, Sivananthan S, Tannock IF. The penetration of anticancer drugs through tumor tissue as a function of cellular adhesion and packing density of tumor cells. Cancer Res. 2006;66(2):1033–9.
5. Kuh HJ, Jang SH, Wientjes MG, Weaver JR, Au JL. Determinants of paclitaxel penetration and accumulation in human solid tumor. J Pharmacol Exp Ther. 1999;290(2):871–80.
6. Tredan O, Galmarini CM, Patel K, Tannock IF. Drug resistance and the solid tumor microenvironment. J Natl Cancer Inst. 2007;99(19):1441–54.
7. Gupta S, Gupta MK. Possible role of nanocarriers in drug delivery against cervical cancer. Nano Rev Exp. 2017;8:1–25.
8. Kijanka M, Dorresteijn B, Oliveira S, van Bergen EN, Henegouwen PM. Nanobody-based cancer therapy of solid tumors. Nanomedicine (Lond). 2015;10(1):161–74.
9. Lee BK, Yun YH, Park K. Smart nanoparticles for drug delivery: boundaries and opportunities. Chem Eng Sci. 2015;125:158–64.
10. Parveen S, Misra R, Sahoo SK. Nanoparticles: a boon to drug delivery, therapeutics, diagnostics and imaging. Nanomedicine. 2012;8(2):147–66.
11. Zeng X, Tao W, Mei L, Huang L, Tan C, Feng SS. Cholic acid-functionalized nanoparticles of star-shaped PLGA-vitamin E TPGS copolymer for docetaxel delivery to cervical cancer. Biomaterials. 2013;34(25):6058–67.
12. Gutierrez-Iglesias G, Hurtado Y, Palma-Lara I, Lopez-Marure R. Resistance to the antiproliferative effect induced by a short-chain ceramide is associated with an increase of glucosylceramide synthase, P-glycoprotein, and multidrug-resistance gene-1 in cervical cancer cells. Cancer Chemother Pharmacol. 2014;74(4):809–17.
13. Lopes-Rodrigues V, Sousa E, Vasconcelos MH. Curcumin as a Modulator of P-Glycoprotein in Cancer: Challenges and Perspectives. Pharmaceuticals. 2016;9(4).
14. Grigore ME. Organic and inorganic Nano-Systems used in Cancer treatment. Journal of Medical Research and Health Education. 2017;1.
15. Duman FD, Erkisa M, Khodadust R, Ari F, Ulukaya E, Acar HY. Folic acid-conjugated cationic Ag2S quantum dots for optical imaging and selective doxorubicin delivery to HeLa cells. Nanomedicine (Lond). 2017;12(19):2319–33.
16. Zhitnyak IY, Bychkov IN, Sukhorukova IV, Kovalskii AM, Firestein KL, Golberg D, et al. Effect of BN nanoparticles loaded with doxorubicin on tumor cells with multiple drug resistance. ACS Appl Mater Interfaces. 2017;9(38):32498–508.
17. Wu GC, Wang ZZ, Bian XS, Du XJ, Wei CH. Folate-modified doxorubicin-loaded nanoparticles for tumor-targeted therapy. Pharm Biol. 2014;52(8):978–82.
18. Sims LB, Curtis LT, Frieboes HB, Steinbach-Rankins JM. Enhanced uptake and transport of PLGA-modified nanoparticles in cervical cancer. Journal of nanobiotechnology. 2016;14:33.
19. Sims LB, Huss MK, Frieboes HB, Steinbach-Rankins JM. Distribution of PLGA-modified nanoparticles in 3D cell culture models of hypo-vascularized tumor tissue. Journal of nanobiotechnology. 2017;15(1):67.
20. Gorodeski GI, Jin W, Hopfer U. Extracellular Ca2+ directly regulates tight junctional permeability in the human cervical cell line CaSki. Am J Phys. 1997;272(2 Pt 1):C511–24.

21. Hoppe-Seyler K, Honegger A, Bossler F, Sponagel J, Bulkescher J, Lohrey C, et al. Viral E6/E7 oncogene and cellular hexokinase 2 expression in HPV-positive cancer cell lines. Oncotarget. 2017;8(63):106342–51.
22. Aasen T, Hodgins MB, Edward M, Graham SV. The relationship between connexins, gap junctions, tissue architecture and tumour invasion, as studied in a novel in vitro model of HPV-16-associated cervical cancer progression. Oncogene. 2003;22(39):7969–80.
23. de la Puente P, Muz B, Gilson RC, Azab F, Luderer M, King J, et al. 3D tissue-engineered bone marrow as a novel model to study pathophysiology and drug resistance in multiple myeloma. Biomaterials. 2015;73:70–84.
24. Ordikhani F, Kim Y, Zustiak SP. The role of biomaterials on Cancer stem cell enrichment and behavior. Jom-Us. 2015;67(11): 2543–9.
25. Filippova M, Filippov V, Williams VM, Zhang K, Kokoza A, Bashkirova S, et al. Cellular levels of oxidative stress affect the response of cervical cancer cells to chemotherapeutic agents. Biomed Res Int. 2014;2014:574659.
26. Steinbach JM, Seo YE, Saltzman WM. Cell penetrating peptide-modified poly(lactic-co-glycolic acid) nanoparticles with enhanced cell internalization. Acta Biomater. 2016;30:49–61.
27. Fahmy TM, Samstein RM, Harness CC, Saltzman WM. Surface modification of biodegradable polyesters with fatty acid conjugates for improved drug targeting. Biomaterials. 2005;26(28):5727–36.
28. Martin DT, Steinbach JM, Liu JC, Shimizu S, Kaimakliotis HZ, Wheeler MA, et al. Surface-modified nanoparticles enhance Transurothelial penetration and delivery of Survivin siRNA in treating bladder Cancer. Mol Cancer Ther. 2014;13(1):71–81.
29. Li J, Feng L, Fan L, Zha Y, Guo L, Zhang Q, et al. Targeting the brain with PEG-PLGA nanoparticles modified with phage-displayed peptides. Biomaterials. 2011;32(21):4943–50.
30. Cu Y, Booth CJ, Saltzman WM. In vivo distribution of surface-modified PLGA nanoparticles following intravaginal delivery. J Control Release. 2011;156(2):258–64.
31. Woodrow KA, Cu Y, Booth CJ, Saucier-Sawyer JK, Wood MJ, Saltzman WM. Intravaginal gene silencing using biodegradable polymer nanoparticles densely loaded with small-interfering RNA. Nat Mater. 2009;8(6):526–33.
32. Beáta Tóth PK, Rémi Magnan. Membrane transporters and transporter substrates as biomarkers for drug pharmacokinetics, pharmacodynamics, and toxicity/adverse events. In: Press A, editor. Biomarkers in Toxicology: Academic Press; 2014. p. 947–963.
33. Kibria G, Hatakeyama H, Akiyama K, Hida K, Harashima H. Comparative study of the sensitivities of cancer cells to doxorubicin, and relationships between the effect of the drug-efflux pump P-gp. Biol Pharm Bull. 2014;37(12):1926–35.
34. Nanayakkara AK, Follit CA, Chen G, Williams NS, Vogel PD, Wise JG. Targeted inhibitors of P-glycoprotein increase chemotherapeutic-induced mortality of multidrug resistant tumor cells. Sci Rep. 2018;8(1):967.
35. Baek N, Seo OW, Kim M, Hulme J, An SS. Monitoring the effects of doxorubicin on 3D-spheroid tumor cells in real-time. Onco Targets Ther. 2016;9:7207–18.
36. Lopez J, Valdez-Morales FJ, Benitez-Bribiesca L, Cerbon M, Carranca AG. Normal and cancer stem cells of the human female reproductive system. Reprod Biol Endocrinol. 2013;11:53.
37. Siadat-Pajouh M, Periasamy A, Ayscue AH, Moscicki AB, Palefsky JM, Walton L, et al. Detection of human papillomavirus type 16/18 DNA in cervicovaginal cells by fluorescence based in situ hybridization and automated image cytometry. Cytometry. 1994;15(3): 245–57.
38. Hoppe-Seyler K, Bossler F, Lohrey C, Bulkescher J, Rosl F, Jansen L, et al. Induction of dormancy in hypoxic human papillomavirus-positive cancer cells. Proc Natl Acad Sci U S A. 2017;114(6):E990–E8.
39. Curtis LT, England CG, Wu M, Lowengrub J, Frieboes HB. An interdisciplinary computational/experimental approach to evaluate drug-loaded gold nanoparticle tumor cytotoxicity. Nanomedicine (Lond). 2016;11(3):197–216.
40. England CG, Gobin AM, Frieboes HB. Evaluation of uptake and distribution of gold nanoparticles in solid tumors. Eur Phys J Plus. 2015;130(11).
41. England CG, Huang JS, James KT, Zhang G, Gobin AM, Frieboes HB. Detection of phosphatidylcholine-coated gold nanoparticles in Orthotopic pancreatic adenocarcinoma using hyperspectral imaging. PLoS One. 2015;10(6):e0129172.
42. Curtis LT, Wu M, Lowengrub J, Decuzzi P, Frieboes HB. Computational modeling of tumor response to drug release from vasculature-bound nanoparticles. PLoS One. 2015;10(12): e0144888.
43. Frieboes HB, Wu M, Lowengrub J, Decuzzi P, Cristini V. A computational model for predicting nanoparticle accumulation in tumor vasculature. PLoS One. 2013;8(2):e56876.
44. van de Ven AL, Abdollahi B, Martinez CJ, Burey LA, Landis MD, Chang JC, et al. Modeling of nanotherapeutics delivery based on tumor perfusion. New J Phys. 2013;15:55004.
45. van de Ven AL, Wu M, Lowengrub J, McDougall SR, Chaplain MA, Cristini V, et al. Integrated intravital microscopy and mathematical modeling to optimize nanotherapeutics delivery to tumors. AIP Adv. 2012;2(1):11208.
46. England CG, Priest T, Zhang G, Sun X, Patel DN, McNally LR, et al. Enhanced penetration into 3D cell culture using two and three layered gold nanoparticles. Int J Nanomedicine. 2013;8:3603–17.
47. Frieboes HB, Edgerton ME, Fruehauf JP, Rose FR, Worrall LK, Gatenby RA, et al. Prediction of drug response in breast cancer using integrative experimental/computational modeling. Cancer Res. 2009;69(10):4484–92.
48. Frieboes HB, Zheng X, Sun CH, Tromberg B, Gatenby R, Cristini V. An integrated computational/experimental model of tumor invasion. Cancer Res. 2006;66(3):1597–604.
49. Froehlich K, Haeger JD, Heger J, Pastuschek J, Photini SM, Yan Y, et al. Generation of multicellular breast Cancer tumor spheroids: comparison of different protocols. J Mammary Gland Biol Neoplasia. 2016;21(3–4):89–98.
50. Comerford KM, Wallace TJ, Karhausen J, Louis NA, Montalto MC, Colgan SP. Hypoxia-inducible factor-1-dependent regulation of the multidrug resistance (MDR1) gene. Cancer Res. 2002;62(12): 3387–94.
51. Rice GC, Hoy C, Schimke RT. Transient hypoxia enhances the frequency of dihydrofolate reductase gene amplification in Chinese hamster ovary cells. Proc Natl Acad Sci U S A. 1986;83(16):5978–82.
52. Rice GC, Ling V, Schimke RT. Frequencies of independent and simultaneous selection of Chinese hamster cells for methotrexate and doxorubicin (adriamycin) resistance. Proc Natl Acad Sci U S A. 1987;84(24):9261–4.